THERMAL EFFICIENCY OF THE PHOTOVOLTAIC-THERMAL AIR-COUPLED PARABOLIC TROUGH-HELIOSTAT CONCENTRATOR (PVT-CCPH)

PASERA Joanès Keneddy[1] , HARITHI BEN Daoud Ben Attoumane[1] , DONA Victorien Bruno[2]

[1]PhD student, Laboratory of Applied Physics and Renewable Energies (LPADER), Ecole Doctoral Génie du Vivant et Modélisation (EDGVM), University of Mahajanga, Madagascar
[2]Professor, Laboratory of Applied Physics and Renewable Energies (LPADER), Ecole Doctoral Génie du Vivant et Modélisation (EDGVM), University of Mahajanga, Madagascar

ABSTRACT

The aim of this study is to optimize the energy performance of the PVT-CCPH hybrid system by harmonizing electrical and thermal efficiency, while controlling the energy required to ensure efficient drying of the product adapted to the climate of the city of Mahajanga. The integration of three solar energy conversion technologies : a photovoltaic-thermal air system (PVT), a parabolic trough concentrator, and a heliostat ensures continuous production of electrical and thermal energy. The PVT hybrid collector is positioned in the focal zone of a parabolic trough concentrator, with a heliostat solar tracking system (PVT-CCPH). This system is designed to produce both electricity and useful heat, specifically for product drying. This configuration represents an advantageous alternative to traditional photovoltaic modules and thermal collectors installed separately. By regulating panel temperature via a cooling system, a balance can be created, harmonizing PVT-CCPH efficiency and thermal output. Using this principle, it is possible to achieve higher electrical efficiency and enough heat to heat air for the dryer. This work therefore involved modeling and simulating this hybrid system using Matlab software. In this study, mathematical models were developed for each component of the system to achieve the desired results.

Keyword : - *Solar irradiation, Air PVT, Fins, Cylindro-Parabolic, Heliostat, Performance, Drying*

1. INTRODUCTION

Hybrid photovoltaic-thermal air collector technology equipped with a Cylindro-Parabolic Concentrator and Heliostat (PVT-CCPH) combines photovoltaic electricity production with the production of hot air from the waste heat behind the solar panels, offering the possibility of improving overall energy efficiency. The underlying idea is simple and effective : by removing heat from the back of the solar panel, hot-air generation improves the efficiency of photovoltaic cells while preventing them from overheating. This is a significant advantage, particularly in climates where temperatures can be high. Madagascar offers considerable advantages for the development of solar energy projects, due to its abundant sunshine and high levels of solar irradiation [1]. However, CPV installations are mainly limited compared with other technologies, and only small CPV plants have been set up for research and demonstration purposes [2,3]. It is in this context that PVT-CCPH technology is emerging as an innovative solution for optimizing

the use of solar energy. The main objective of this study is to improve the energy performance of the hybrid solar photovoltaic-thermal air collector equipped with a Cylindro-Parabolic Concentrator and Heliostat (PVT-CCPH) by seeking a balance between electrical and thermal efficiency, while minimizing the energy required for the drying process. Parabolic trough concentrators with heliostats efficiently collect solar radiation without a tracking system. However, they raise the temperature of the PV cells, reducing their efficiency. Aluminum fins are used for cooling, and the hot air generated is used for drying. Matlab was used to model and simulate this hybrid system using mathematical models.

2. METHODOLOGIES

2.1. System configuration

The PVT hybrid air collector consists of several layers: glass, PV cells, EVA film, tedlar, finned top absorber, heat transfer air, bottom absorber and thermal insulation. It is placed between two reflectors, first receiving the radiation reflected by the heliostat, which directs it to the parabolic trough concentrator, regardless of the sun's position [3,4,5]. This parabolic trough then focuses the solar energy on the focal line where the PVT is located [3,6].

The PVT uses concentrated solar radiation to generate electricity and heat by extracting hot air from beneath the photovoltaic cells. In the event of low solar irradiation, a thermal booster heats the air to the temperature required for optimum drying. The hot air is then distributed evenly throughout the drying chamber by a fan, with or without the help of the booster. The auxiliary unit is supplied with direct current via a battery and a charge controller.

MPPT control continuously optimizes the electrical load to maximize energy output, despite variations in irradiance and temperature [7]. The boost converter (DC-DC) adjusts the output voltage by modifying the duty cycle [3]. The battery stores the energy to power the inverter, guaranteeing power even in the absence of the main source, such as the PVT. The inverter (DC-AC) converts battery energy into AC voltage to power AC loads.

The figure below shows the configuration of a hybrid concentrating solar collector.

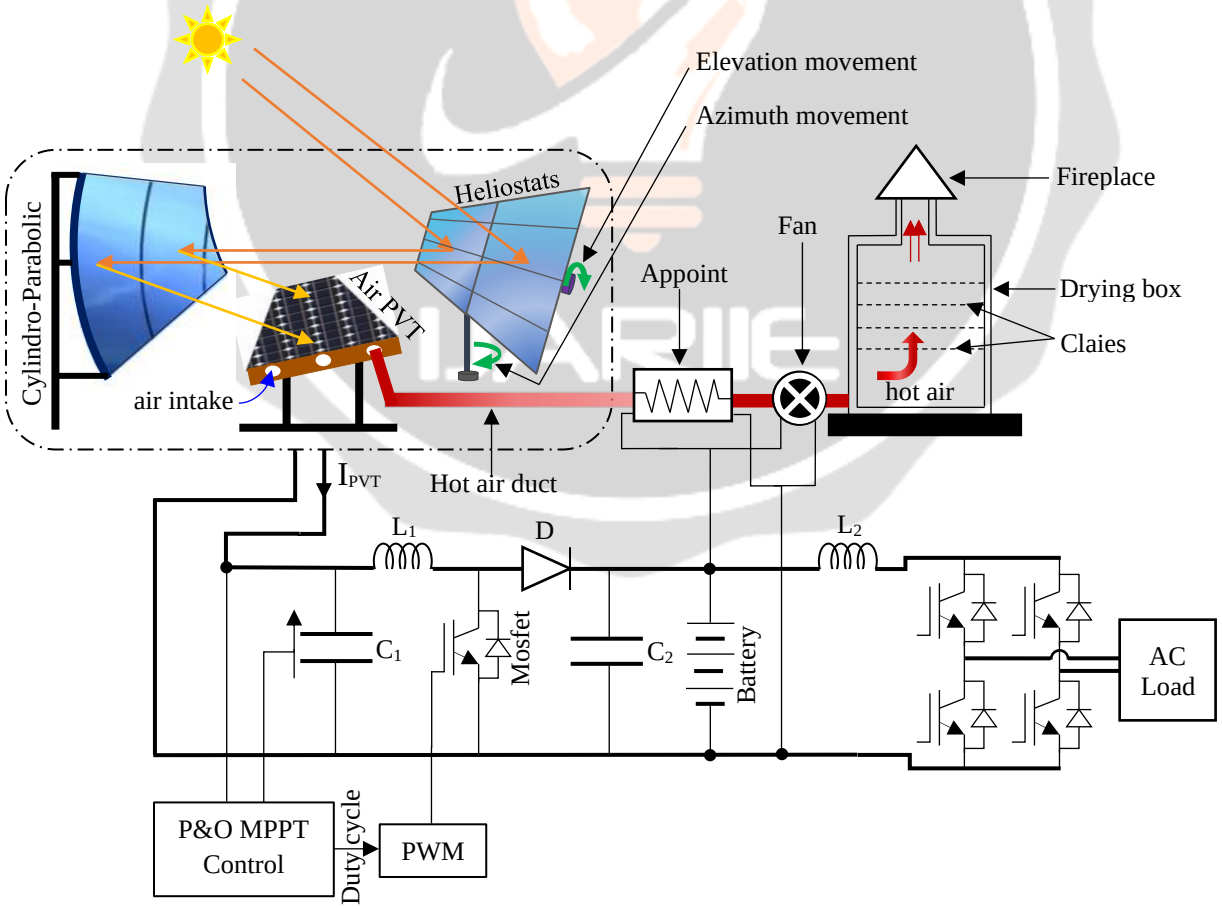

Fig-1: System configuration PVT-CCPH

2.1.1 Mathematical modeling

A cross-section of a PVT hybrid air collector is shown in Figure 2 [8,9,10].

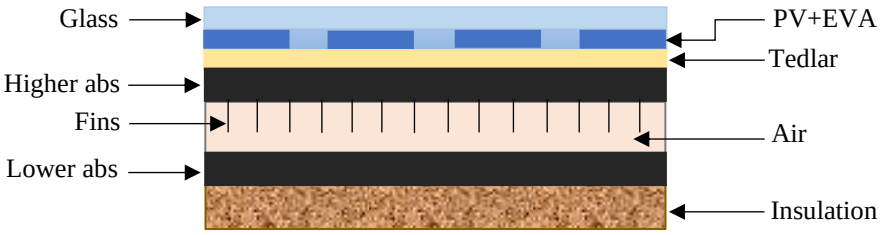

Fig-2 : Cross-section of PVT hybrid air collector.

Figure 3 shows the equivalent electrical circuit of the PVT hybrid air collector.

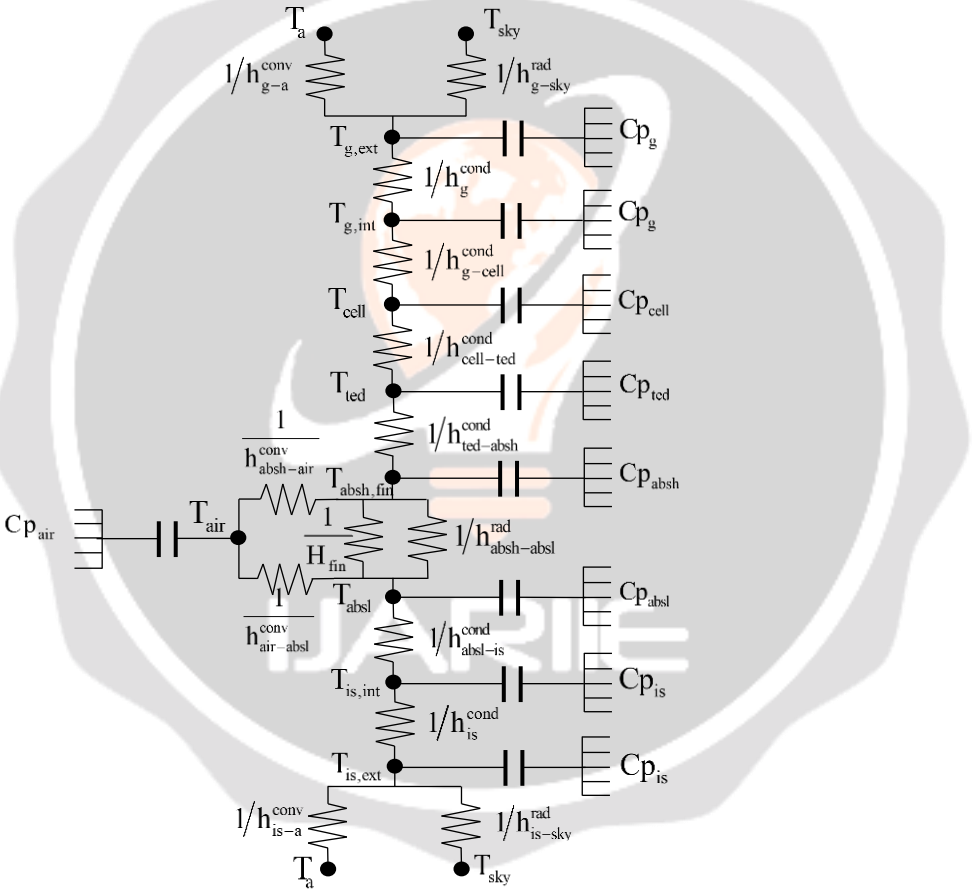

Fig-3 : Equivalent electrical circuit of the PVT hybrid air collector [11,12].

2.1.2 Study hypothesis

Certain calculation assumptions must be defined before modelling can begin [3,8,9,10,13,14] :

- The sky can be assimilated to a black body with an equivalent temperature calculated ;
- Heat transfer is considered to be one-dimensional through the layers of the system ;
- The ambient temperature is the same around the sensor ;

- The floor temperature is taken to be equal to the ambient temperature ;
- EVA's transmission coefficient is 100% ;
- Mass flow is uniform in the air layer duct;
- The wind speed on the face of the collector is assumed to be constant ;
- The thermo-physical properties of the fluid are a function of temperature ;
- The absorber's thermal and geometric properties are equal ;
- The thermal properties of the fin are equal to those of the absorber ;
- The effect of shading and dust on the collector is negligible ;
- Heliostat concentration is equal to one.

2.1.3 Equating the system

The following equations were obtained by applying Ohm's law to the mesh node from the equivalent circuit shown in figure 3 [8,9,10,11,14,15] :

Node 1 : outer face of glass

$$\frac{m_g Cp_g}{S_g}\left(\frac{dT_{g,ext}}{dt}\right) = G_i \cdot C - h_{g-a}^{conv}\left(T_{g,ext} - T_a\right) - h_g^{cond}\left(T_{g,ext} - T_{g,int}\right) - h_{g-sky}^{rad}\left(T_{g,ext} - T_{sky}\right) \quad (01)$$

Node 2 : inner face of glass pane

$$\frac{m_g Cp_g}{S_g}\left(\frac{dT_{g,int}}{dt}\right) = \alpha_g \cdot G_i \cdot C + h_g^{cond}\left(T_{g,ext} - T_{g,int}\right) - h_{g-cell}^{cond}\left(T_{g,int} - T_{cell}\right) \quad (02)$$

Node 3 : PV cell

$$\frac{m_{cell} Cp_{cell}}{S_{cell}}\left(\frac{dT_{cell}}{dt}\right) = \tau_g \cdot \alpha_{cell} G_i \cdot C + h_{g-cell}^{cond}\left(T_{g,int} - T_{cell}\right) - h_{cell-ted}^{cond}\left(T_{cell} - T_{ted}\right) - \frac{Q_{élec}}{S_{cell}} \quad (03)$$

Node 4 : tedlar layer

$$\frac{m_{ted} Cp_{ted}}{S_{ted}}\left(\frac{dT_{ted}}{dt}\right) = h_{cell-ted}^{cond}\left(T_{cell} - T_{ted}\right) - h_{ted-absh}^{cond}\left(T_{ted} - T_{absh}\right) \quad (04)$$

Node 5 : top absorber layer and fins

$$\frac{m_{abs} Cp_{abs}}{S_{abs}}\left(\frac{dT_{absh}}{dt}\right) = h_{cell-absh}^{cond}\left(T_{ted} - T_{absh}\right) - h_{absh-air}^{conv}\left(T_{absh} - T_{air}\right) - H_{fin}\left(T_{absh} - T_{air}\right) - h_{absh-absl}^{rad}\left(T_{absh}^4 - T_{absl}^4\right) \quad (05)$$

With [8,16] : $H_{fin} = h_{absh-air}^{conv}.N.\eta_{fin}.S_t$ (06)

With : $\eta_{fin} = \dfrac{\tanh\left(L_c \cdot \sqrt{\dfrac{P.h_{fin}^{conv}}{\lambda_{fin} e_{fin}}}\right)}{L_c \cdot \sqrt{\dfrac{P.h_{fin}^{conv}}{\lambda_{fin}.e_{fin}}}}$ $S_t = N.\left(2.H_c.L_c\right) + S$, $L_c = L + \dfrac{e_{fin}}{2}$ and $P = 2\left(L + e_{fin}\right)$ (07)

Where : S_t , L_c , P and e_{fin} are respectively the total available surface area, corrected length, perimeter and thickness of a fin.

Node 6 : air layer

$$\frac{m_{air} Cp_{air}}{S_{air}}\left(\frac{dT_{air}}{dt}\right) = h_{absh-air}^{conv}\left(T_{absh} - T_{air}\right) + H_{fin}\left(T_{absh} - T_{air}\right) + h_{air-absl}^{conv}\left(T_{absl} - T_{air}\right) - \dot{m} Cp_{air}\left(T_{air,out} - T_{air,int}\right) \quad (08)$$

Node 7 : lower absorber layer

$$\frac{m_{absl} Cp_{absl}}{S_{abB}}\left(\frac{dT_{absl}}{dt}\right) = h_{air-absl}^{conv}\left(T_{air} - T_{absl}\right) - h_{absl-is}^{cond}\left(T_{absl} - T_{is,int}\right) + h_{absh-absl}^{rad}\left(T_{absh}^4 - T_{absl}^4\right) \quad (09)$$

Node 8 : inside face of insulation

$$\frac{m_{is}Cp_{is}}{S_{is}}\left(\frac{dT_{is,int}}{dt}\right)=h_{absl-is}^{cond}\left(T_{absl}-T_{is,int}\right)-h_{is}^{cond}\left(T_{is,int}-T_{is,ext}\right) \quad (10)$$

Node 9 : outer face of insulation

$$\frac{m_{is}Cp_{is}}{S_{is}}\left(\frac{dT_{is,ext}}{dt}\right)=h_{is}^{cond}\left(T_{is,int}-T_{is,ext}\right)-h_{is-a}^{conv}\left(T_{is,ext}-T_{a}\right)-h_{is-sol}^{rad}\left(T_{is,ext}-T_{sol}\right) \quad (11)$$

2.1.4 Heat exchange coefficients

❖ **Conductive heat transfer coefficient**

In general, the conductive heat transfer coefficient between two layers of adjacent components m_i and n_i is given by the empirical relationship as follows [9] :

$$h_{m_i-n_i}^{cond}=\left(\frac{e_{m_i}}{\lambda_{m_i}}+\frac{e_{n_i}}{\lambda_{n_i}}\right)^{-1} \quad (12)$$

❖ **Convective heat transfer coefficients** [8,9].

The Mac Adams correlation was used to determine the heat exchange between the glass and the environment :

$$h_{v-a}^{conv}=5,6+3,8V_{vent} \text{ where } V_{vent} \text{ is the wind speed.} \quad (13)$$

Convective heat exchange coefficients are calculated using empirical correlations based on the Nusselt number :

$$h_{air}^{conv}=\frac{N_u\lambda_{air}}{D_h} \quad (14)$$

Heat transfer between absorber and fluid :

$$h_{abs-air}^{conv}=\left(\frac{e_{abs}}{\lambda_{abs}}+\frac{1}{h_{air}^{conv}}\right)^{-1} \quad (15)$$

In our case, the Nusselt number is calculated according to the flow regime, which is expressed by the following equations [17,18] :

- For laminar flow $\left(Re_{air}<2300\right)$

$$Nu=N_{\infty}+\frac{a\left[Pr_{air}\cdot Re_{air}\cdot D_h/L\right]^{m'}}{1+b\left[Pr_{air}\cdot Re_{air}\cdot D_h/L\right]^{n'}} \text{ (Heaton's empirical correlation)} \quad (16)$$

With : $a=0.00190,\ b=0.00563,\ N_{\infty}=5.4,\ Pr=0.7,\ n'=1.17,\ m'=1.71$

- For transient flow $\left(2300<Re_{air}<6000\right)$

$$Nu=0.0214\times\left(Re_{air}^{0.8}-100\right)\times Pr_{air}^{0.4}\times\left[1+\left(D_h/L\right)^{0.66}\right] \quad (17)$$

With conditions : $0.5\le Pr_{air}\le 1.5$ $2300<Re_{air}<10^6$ and $0<D_h/L<1$

- For turbulent flow $\left(Re_{air}>6000\right)$

$$Nu=0.023\times\left(Re_{air}\right)^{0.8}\times\left(Pr_{air}\right)^{0.4} \text{ (the empirical correlation of Tan and Charters (1970)).} \quad (18)$$

With : $0.6\le Pr_{air}\le 160$ $Re_{air}\ge 10000$ and $L/D_h\ge 10$

The Prandtl and Reynolds number is defined by the following relationship [9] :

$$Pr_{air} = \frac{\mu_{air}.Cp_{air}}{\nu_{air}} \text{ and } Re_{air} = \frac{V_{air}D_h}{\nu_{air}} \text{ , with } D_h = \frac{4(l \times H_c)}{2(l + H_c)} \quad (19)$$

Where : D_h , ℓ and H_c are hydraulic pipe diameter, sensor width and air pipe height respectively.

- **Coefficient of radiant heat exchange** [8,9,10].

The radiative exchange coefficient is calculated using empirical formulas as follows :

$$h^{rad}_{g-sky} = \varepsilon_g.\sigma.\left(T_{g,ext} + T_{sky}\right)\left(T^2_{g,ext} + T^2_{sky}\right) \quad (20)$$

$$h^{rad}_{absh-absl} = \sigma\frac{\left(T_{absh} + T_{absl}\right)\left(T^2_{absh} + T^2_{absl}\right)}{\left(\frac{1}{\varepsilon_{absh}}\right) + \left(\frac{1}{\varepsilon_{absl}}\right) - 1} \quad (21)$$

Where: $\sigma = 5,67 \times 10^{-8}$, Stephan Boltzmann's constant ;

$T_{sky} = 0,0552.(T_a)^{1,5}$, the temperature of the sky is given by the Swinbank relation.

With : $T_a = \left[\frac{T_{a\ max} - T_{a\ min}}{2}\right].\cos\left[\frac{(TSV - 12).\pi}{12}\right] + \left[\frac{T_{a\ max} + T_{a\ min}}{2}\right]$ ambient temperature.

The physical properties of air are assumed to vary linearly with temperature. Specific expressions have been given by Ebrahim and Alfege [10] :

- Specific gravity: $\rho_{air} = 1.1774 - 0.000359 \times T_{air}$;
- Specific heat: ; $Cp_{air} = [1.0057 + 0.000066 \times T_{air}] \times 1009$
- Thermal conductivity: $\lambda_{air} = 0.02624 + 0.0000758 \times T_{air}$;
- Dynamic viscosity: $\mu_{air} = [1.983 + 0.00184 \times T_{air}] \times 10^{-5}$.

2.2 Concentric Cylindro-Parabolic (CCP) solar collector

Uniformity of irradiance at the CCP outlet is essential. Energy concentration is the ratio between the average irradiance on the PVT absorber (Gr) and the direct irradiance received at the CCP opening (Go). The geometric concentration ratio corresponds to the ratio between the surface area of the CCP opening and that of the receiver [6,19].

$$C = \frac{G_r}{G_o} = C_g \times \rho_{ccp} \times \cos(\theta_{inc}) \text{ and } C_g = \frac{A_o}{A_r} = \frac{W_o}{W_r \times \cos(\theta_{inc})} = \frac{4 \times f \times \tan(\theta_o/2)}{W_r \times \cos(\theta_{inc})} \quad (22)$$

Where : $\rho_{ccp}, \theta_{inc}, \theta_o, W_o$ and f represent collector reflectivity, concentrator aperture width, angle of incidence, aperture angle, focal length.

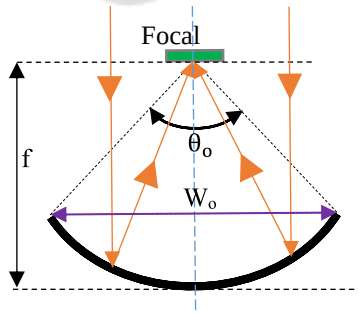

Fig-4 : Cross-section of a CCP [4].

2.3 PVT hybrid air collector performance

The power, electrical and thermal respectively, produced by the PVT hybrid solar collector are given by the following equation [9,14] :

$$Q_{élec} = \tau_g . G_i . C . S_{cell} . \eta_{ref} . \exp\left[\beta\left(T_{cell} - T_{ref}\right)\right] \text{ and } Q_{the} = \dot{m} . Cp_{air} . \left(T_{air,out} - T_{air,int}\right) \quad (23)$$

Where : G_i is global solar irradiance.

The efficiency, electrical and thermal respectively, of the PVT hybrid collector are obtained by the following two expressions [8,9,18].

$$\eta_{elc} = \frac{Q_{elec}}{S_{cell} \cdot G_i \cdot C} \text{ and } \eta_{the} = \frac{Q_{the}}{S_{cell} \cdot G_i \cdot C} \quad (24)$$

The overall PVT efficiency is the sum of the thermal efficiency and the thermal efficiency equivalent to the electrical efficiency [9,18].

$$\eta_{PVT} = \eta_{the} + \eta_{elec,the} \quad (25)$$

With : $\eta_{elec,the} = \frac{\eta_{elec}}{C_f}$ where C_f is the thermal energy conversion factor between 0.35 and 0.4.

3. RESULTS AND DISCUSSION

The study area, Mahajanga, located in northwest Madagascar (15°43' S, 46°19' E), has meteorological data from ASECNA analyzed over 14 years (2010-2023). The Page model was used to estimate solar irradiance [21,22,23].

The photovoltaic collector, made of polycrystalline silicon, has the parameters detailed in Table 1. Its performance has been assessed in accordance with international standards, under standard conditions: irradiation of 1000 $W.m^{-2}$, spectrum AM 1.5 and temperature 25 °C.

Table-1: Electrical characteristics of a KC200GT photovoltaic module [7].

Experimental peak power P_{max}	200 W
Voltage at point of maximum power V_{pm}	26.3 V
Current at point of maximum power I_{pm}	7.61 A
Open circuit voltage V_{oc}	32.9 V
Short-circuit current I_{sc}	8.21 A
Voltage temperature coefficient k_v	–0.123 V/°C
Current temperature coefficient k_i	0.00318 A/°C
Operating temperature	–40 °C to +85 °C
Number of cells in series N_s	54
Number of parallel cells N_p	1
Reference yield	15 %
Dimension $(L \times l \times h)$	1425 mm × 990 mm × 36 mm

Table 2 shows the characteristics of the various sensor components.

Table-2: Features of PVT hybrid module components **[10]**.

	Components		
Features	Glass coating	PV cell	Layer of tedlar
Density	2200 $Kg.m^{-3}$	2330 $Kg.m^{-3}$	1390 $Kg.m^{-3}$
Specific heat	670 $J.Kg^{-1}K^{-1}$	836 $J.Kg^{-1}K^{-1}$	1400 $J.Kg^{-1}K^{-1}$
Thermal conductivity	0.93 $W.K^{-1}.m^{-1}$	148 $W.K^{-1}.m^{-1}$	0.033 $W.K^{-1}.m^{-1}$
Glazing emissivity	0.88	0.93	0.88
Thickness	0.004 m	0.0003 m	0.0005 m
Absorption coefficient	0.066	0.85	0.5

Features	Absorber	Insulation
Density	8000 $Kg.m^{-3}$	2200 $Kg.m^{-3}$
Specific heat	36 $J.Kg^{-1}K^{-1}$	670 $J.Kg^{-1}K^{-1}$
Thermal conductivity	410 $W.K^{-1}.m^{-1}$	0.93 $W.K^{-1}.m^{-1}$
Glazing emissivity	0.04	0.88
Thickness	0.0005 m	0.004 m
Absorption coefficient	0.75	0.066

3.1 Variation in solar irradiation and ambient temperature at Mahajanga

Figure 5 shows the simulated evolution of monthly mean hourly irradiance and ambient temperature over the course of the day of October 15, over the last 14 years. The figure shows that solar irradiance and ambient temperature both increase as the day progresses. Solar irradiance begins to rise in the morning, peaking at around 940 $W.m^{-2}$ around midday, before gradually falling back in the afternoon. Ambient temperature peaks slightly later. This time lag in relation to the irradiation peak is due to the thermal inertia of materials, their heat storage capacity and heat transfer processes, which are slower than the evolution of solar irradiation. The ambient temperature reaches a maximum of 32.92 °C at 12.8 h, corresponding to the hottest moment of the day. This figure also shows that the temperature is lower in the morning than at the end of the day.

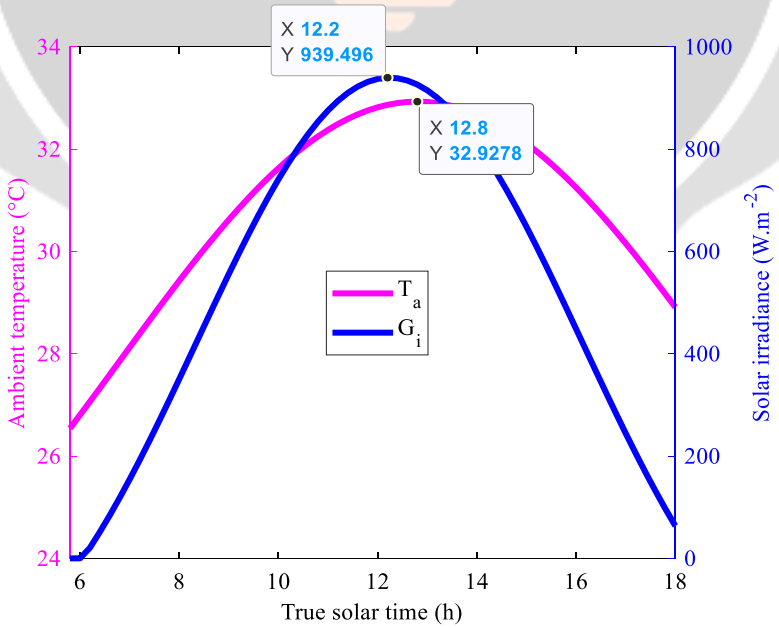

Fig-5: Temporal variation in solar irradiance and ambient temperature.

3.2 Simulation of a parabolic trough concentrator

Figure 6 illustrates the evolution of energy concentration over the course of the day, as a function of the geometric concentration ratio, the angle of incidence of the sun's rays and the optical properties of the materials, including their reflectivity. This figure shows that energy concentration follows the same trend as solar irradiance, with a peak in energy around midday. As the geometric concentration ratio increases, energy concentration rises, reaching a maximum value of 1.79 for Cg = 2. These results enable us to assess the actual intensity of the energy captured and used by the PVT sensor. Thanks to the heliostat, solar radiation always remains perpendicular to the surface of the parabolic trough concentrator (CCP), ensuring a zero angle of incidence (0°). This configuration enables the collector to maintain optimum performance throughout the day, without any shading effects. Combining the heliostat with the CCP maximizes optical performance, guaranteeing efficient and constant capture of solar energy.

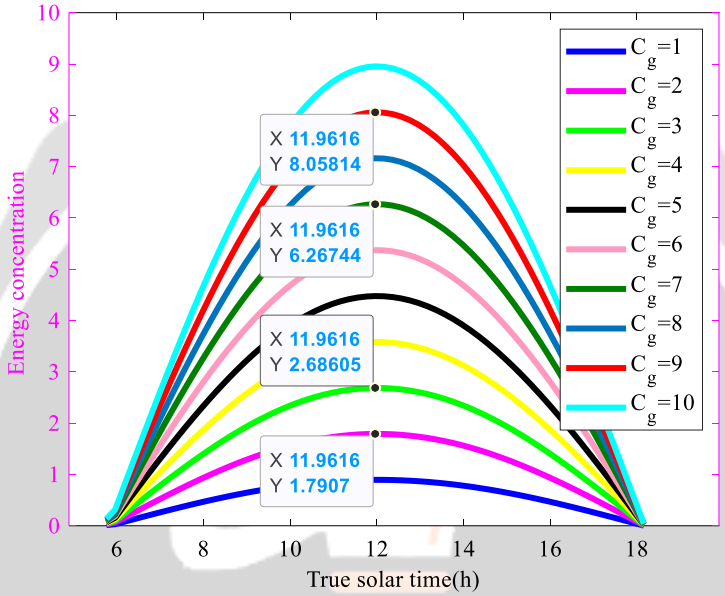

Fig-6 : Energy consultation

3.3 PVT hybrid collector element temperature

Figure 7 shows the temperature distribution in the different layers of the PVT air collector as a function of time. For the month of October at the Mahajanga site, layer temperatures increase progressively as solar irradiation intensifies during the day, reaching their maximum around midday. These results were obtained without the use of a solar concentration system and in the absence of fins, with an air flow rate of 0.02 $Kg.s^{-1}$ and an air layer thickness of 0.03 m. The solar cell temperature stands out as the highest, reaching around 55.98 °C. However, the temperatures of the tedlar and top absorber are very close to those of the solar cells, at 55.84 °C and 55.70 °C respectively. This highlights the efficient heat transfer between the photovoltaic cells and the absorber plate, enabling the heat accumulated by the cooling fluid to be dissipated. Finally, the curves obtained are in line with the experimental data reported by TOUAFEK Khaled [9].

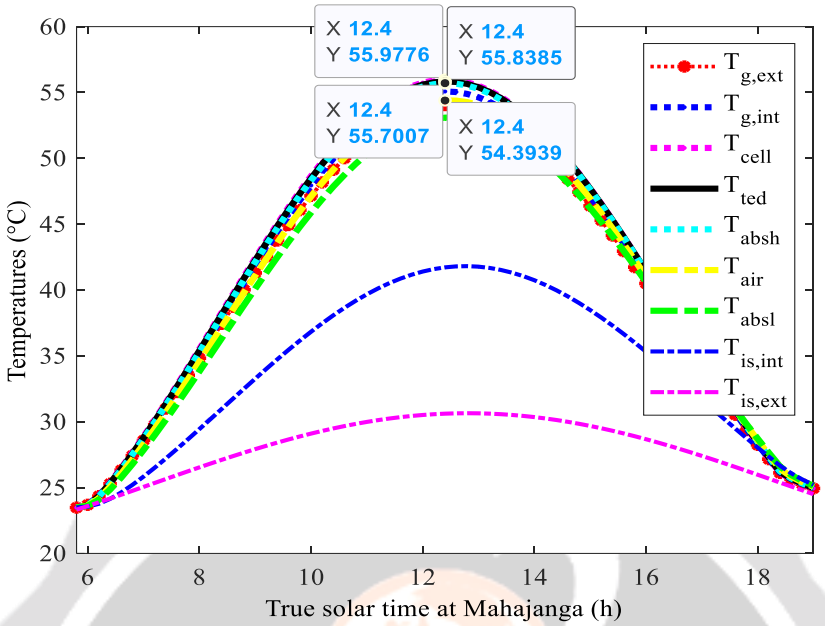

Fig-7 : Temperature variation of the various components of the PVT hybrid air collector.

3.5 Energy performance of the PVT-CCPH system

Figure 8 illustrates the evolution of the electrical and thermal performance of the PVT-CCPH system with solar concentration (C = 2) as a function of time and the number of fins (N). The simulations, carried out with an air mass flow rate of 0.02 $Kg.s^{-1}$, an air layer height of 0.03 m and a fin thickness of 0.005 m, show that electrical power follows the variation in solar irradiation, peaking around midday before gradually decreasing in the afternoon. The addition of fins improves the cooling of photovoltaic cells by increasing heat dissipation, thereby maintaining their efficiency. However, beyond a certain threshold (N = 30), the improvement becomes negligible due to thermal saturation.

Thermal output increases with the number of fins, as they enlarge the heat exchange surface between the absorber plate and the air. However, this increase eventually stabilizes at a high number of fins, as the reduced space between them limits the efficient circulation of the heat transfer fluid. This phenomenon also affects thermal efficiency, which follows a similar trend, reaching saturation at the same threshold. On the other hand, electrical efficiency decreases slightly with a high number of fins, due to less efficient air flow and reduced heat exchange.

These results show that a moderate number of fins is essential to balance electrical and thermal performance. Too many fins can reduce efficient air circulation, leading to insufficient cooling of PV cells and thermal stagnation. An optimal compromise for the system requires consideration of the interactions between fin number, mass flow rate, wind speed, air layer height and fin thickness to maximize the overall performance of the PVT-CCPH system.

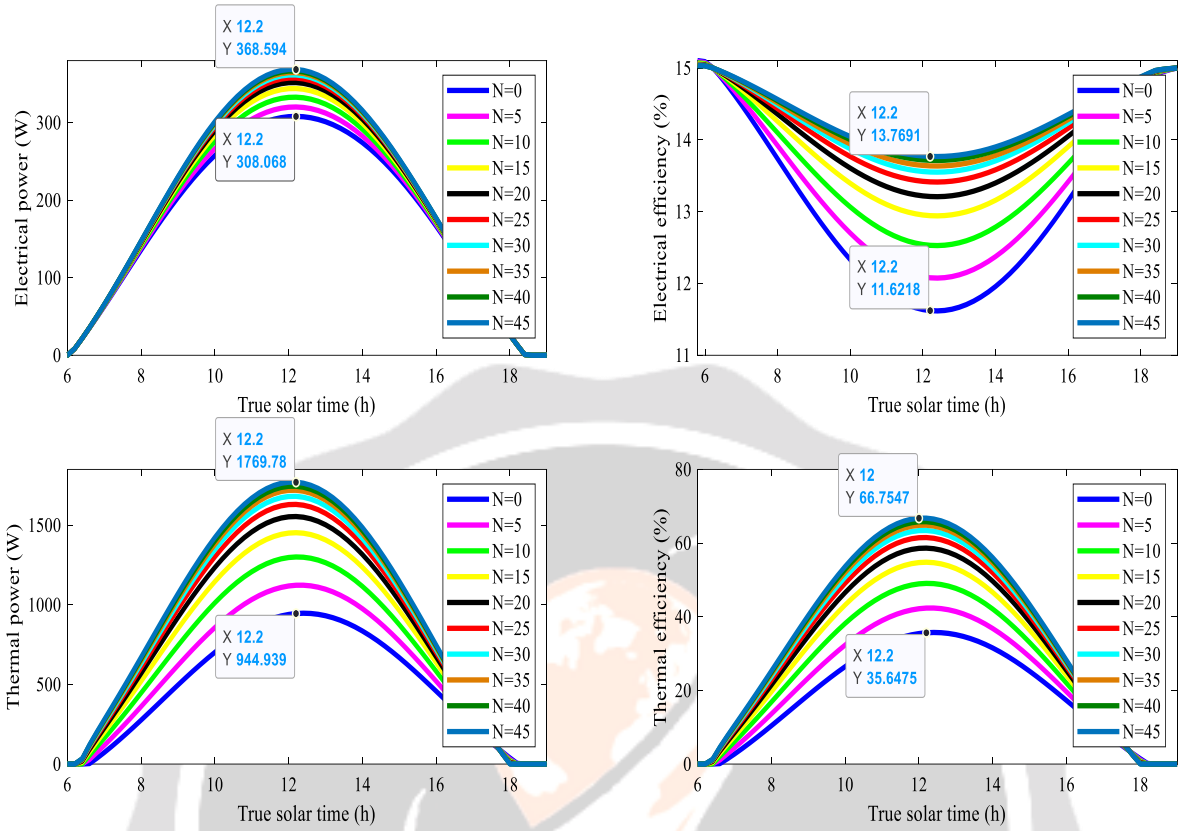

Fig-8 : Impact of the number of fins on the energy performance of an air-cooled PVT system with solar concentration (C = 2).

3.6 Variation in PVT-CCPH mass airflow and wind speed

Figure 9a shows the evolution of the thermal efficiency of the PVT-CCPH system over the course of the day for different air mass flow rates (m_a). The choice of a moderate number of fins (N = 22) and a thickness of 0.005 m offers a balance between efficient heat dissipation and low resistance to airflow. With a fin spacing of 0.042 m, airflow is sufficiently fluid to avoid excessive resistance, while maintaining moderate turbulence to promote heat transfer. What's more, the high thermal conductivity of the rectangular aluminium fins efficiently dissipates heat to the air, reducing the temperature of the photovoltaic cells. This figure also confirms that thermal efficiency increases as air mass flow rate rises, showing that higher flow rates promote more efficient cooling, optimizing both electrical efficiency and useful heat recovery, while ensuring stable overall system performance.

Wind speed (Fig. 9b) improves the thermal efficiency of the PVT-CCPH. A higher wind speed means faster dissipation of the heat accumulated on the surface of the PV cells. This reduces their temperature, thus increasing their electrical efficiency. On the other hand, increasing wind speed has a negative impact on the system's thermal efficiency. This figure also shows that reducing the wind speed, such as 3 m. s^{-1} , increases the system's thermal efficiency, while increasing it decreases it. It can be seen that when the wind speed exceeds 6 $m.s^{-1}$, the thermal efficiency begins to decrease slightly. This is due to excessive heat dissipation and turbulence, which reduce heat transfer efficiency.

These results show that high airflows and moderate wind speeds (between 3 $m.s^{-1}$ and 5 $m.s^{-1}$) optimize the thermal performance of the system.

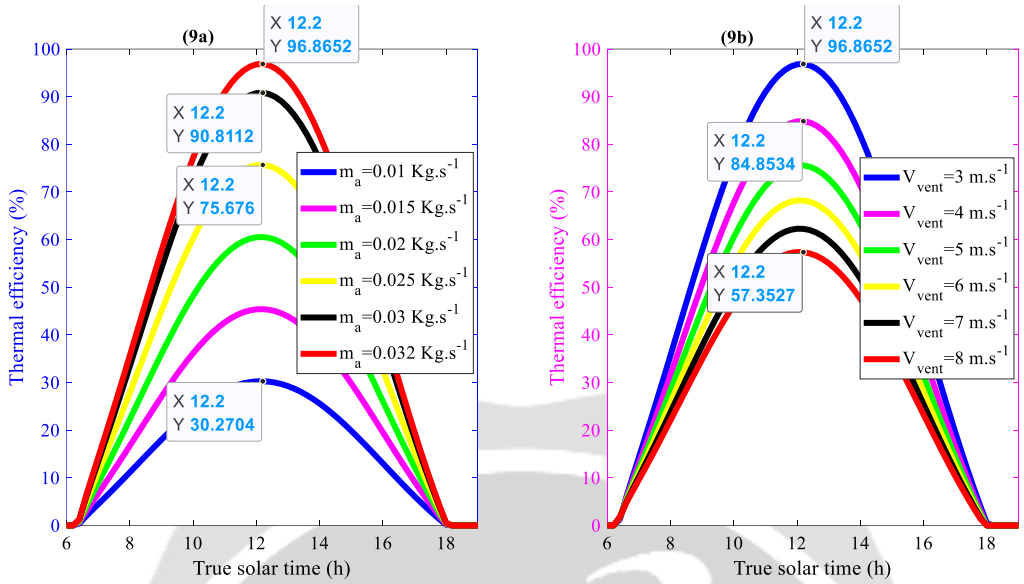

Fig-9 : Temporal evolution of thermal efficiency as a function of air mass flow rate and wind speed.

3.7 Varying the height and thickness of PVT-CCPH fins

Figure 10 shows the thermal efficiency of the PVT-CCPH system over the course of the day as a function of two parameters (fin height and fin thickness). Figure 10a shows that thermal efficiency increases with fin height. This is because higher fins allow a larger heat exchange surface, improving heat dissipation and keeping the photovoltaic cells at lower temperatures. Figure 10a also shows that from a height of 0.03 m, the gap between the curves decreases, indicating that the effect of increasing height becomes less significant.

Figure 10b shows that thermal efficiency also increases with increasing fin thickness. This can be explained by the fact that increasing fin thickness increases thermal conductivity, enabling more efficient heat transfer from the absorber plate to the air.

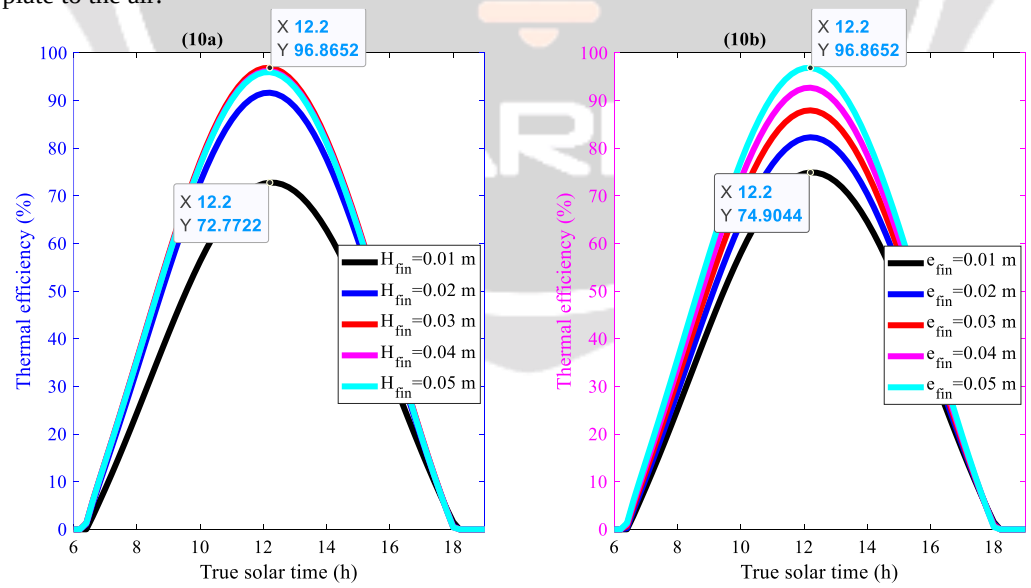

Fig-10 : Temporal evolution of thermal efficiency as a function of fin height and thickness

3.8 Cell and air temperature variation in a PVT-CCPH with moderate parameters

The curves in Figure 11 show the temporal variations in cell and air temperatures with moderate PVT-CCPH system parameters. The moderate parameters chosen for the PVT are : number of fins (N = 22), fin thickness (e_{fin} = 0.005 m), air mass flow rate (m_a = 0.028 Kg.s^{-1}), air layer height (H_c = 0.03 m) and a fin spacing of (0.042 m). The results demonstrate optimum system performance. The maximum cell temperature reached 50.95 °C with a solar concentration of C = 2, compared with 40.41 °C without concentration, demonstrating the system's efficiency in capturing more solar energy. In addition, the air temperature reaches 110.42 °C with concentration, compared with 70.53 °C without concentration, guaranteeing high heat output, ideal for thermal applications such as drying. These results show that the system delivers excellent simultaneous power and heat production, while making effective use of selected configurations, such as fin spacing and airflow, to maximize performance.

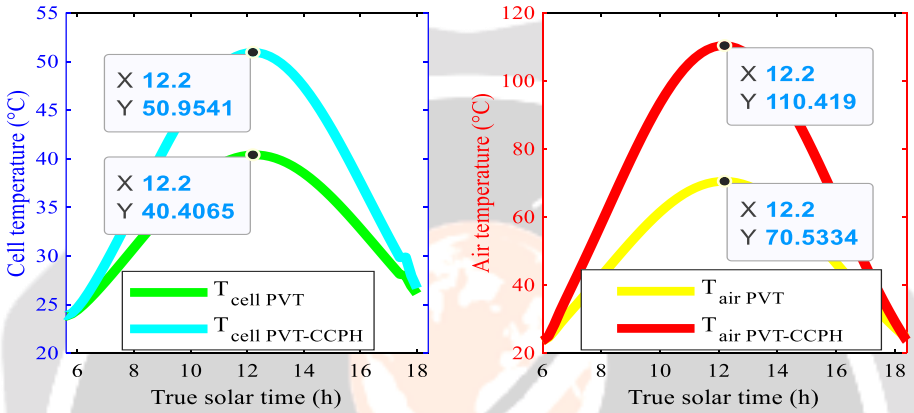

Fig-11 : Evolution of cell and air temperatures with and without concentration as a function of time.

3.9 Energy performance of the PVT-CCPH system with moderate parameters

Figure 12 illustrates the efficiency of the PVT-CCPH system as a function of the optimized parameters. These results highlight the excellent balance between electrical and thermal production of the PVT-CCPH system, demonstrating optimum performance throughout the solar day. Stable electrical efficiency, reaching 13.35 %, combined with high thermal efficiency, results in a remarkable overall efficiency of 98 %. This performance was achieved with a solar concentration of C = 2, illustrating highly efficient conversion of solar energy, suitable for combined applications such as generating electricity to power equipment and supplying heat for thermal uses such as drying. The design, including optimal fin spacing, fin thickness, well-tuned airflow and adequate air layer height, ensures smooth operation and maximum valorization of captured energy, making this system a versatile, high-performance solution for energy needs.

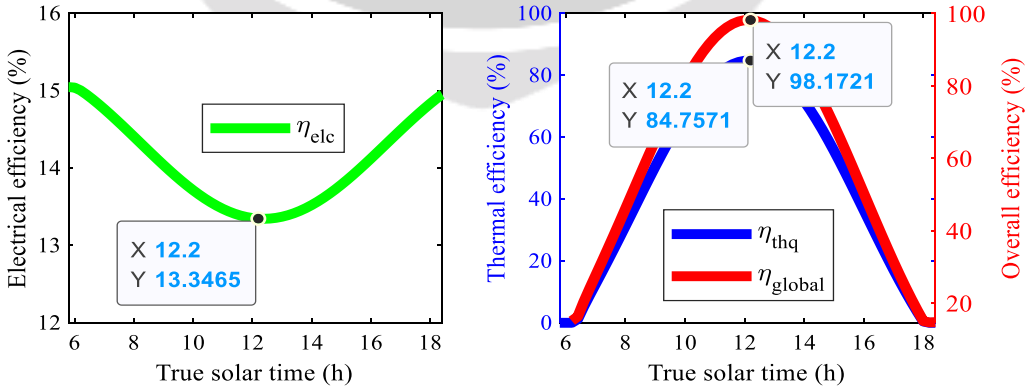

Fig-12 : PVT-CCPH system efficiency as a function of moderated parameters

3.10 Thermal performance of PVT and PVT-CCPH systems with moderate parameters

Figure 13 illustrates the thermal efficiency of a photovoltaic-thermal (PVT) system alone and a PVT system coupled with a parabolic trough concentrator and heliostat (PVT-CCPH), as a function of optimized parameters and solar time. Both systems reach their peak efficiency at 12.2 h, where the PVT-CCPH performs slightly better (84.76 %) than the PVT alone (82.33 %), thanks to the concentration of solar radiation increasing heat collection. At the beginning and end of the day (6 a.m. and 6 p.m.), the thermal efficiencies of the two systems converge towards 0 %, due to low solar irradiation. Overall, the PVT-CCPH system shows a slightly higher thermal efficiency and may offer advantages for applications requiring increased and optimized heat collection during periods of high solar irradiation.

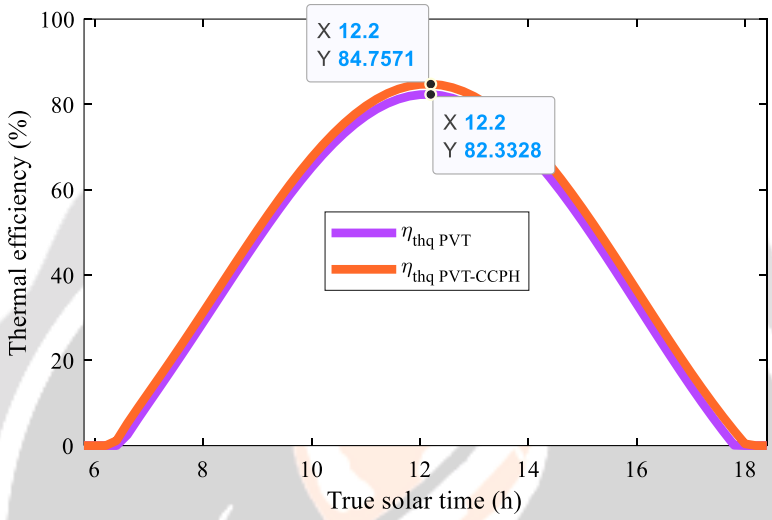

Fig-13 : Time variation in thermal efficiency of PVT and PVT-CCPH systems

4. CONCLUSION

The work presented in this article concerns the study and improvement of the thermal performance of a PVT hybrid system coupled with a parabolic trough concentrator and a heliostat (PVT-CCPH). The main drawback of PVT solar collectors is their conversion efficiency. Indeed, a large proportion of solar irradiance is not converted into energy (electrical or thermal) due to reflection losses and/or heating (increased solar cell temperature). The integration of solar reflectors reduces reflection losses, while the incorporation of heat exchangers by assembling fins under the cells ensures their cooling, and therefore minimizes thermal losses. Improving the performance of the PVT-CCPH relies on the optimization of several factors : the number, thickness and spacing of the fins, the air mass flow rate, the height of the air layer, and the wind speed. Numerical simulations reveal that adjustments to parameters such as excessively high air flow, excessive wind speed or too deep an air channel are necessary to avoid a drop in performance. The optimum configuration was identified for 22 fins 0.005 m thick, spaced 0.042 m apart, with an air mass flow rate of 0.028 $Kg.s^{-1}$ and an air channel height of 0.03 m. These optimized parameters make it possible to maintain a PV module temperature of 50 °C and achieve an air temperature of 110.42 °C under solar concentration (compared with 70.53 °C without concentration). The system achieves a stable thermal efficiency of 84.76 %, effectively balancing electricity and heat production for applications such as drying.

5. REFERENCES

[1]. DONA Victorien Bruno, 'Modélisation et conversion des irradiations solaires en vue de la production d'énergie renouvelable à Mahajanga' Habilitation to direct research, University of Mahajanga, Madagascar, August 28, 2019.
[2]. El-YAHYAOUI Sara. 'Concentrated photovoltaics: optimization of the secondary stage', cotutelle thesis, Université Sidi Mohamed Ben Abdellah & Université de Lorraine, March 26, 2021.
[3]. Olfa Bel Haj Brahim Kechiche, 'Concentrator Photovoltaic (CPV): Maximum Power Point Techniques (MPPT) Design and Performance', Unversity of sousse, researchgate, 2021.
[4]. BOUAMRA M. 'Etude de la distribution du flux au foyer d'une centrale solaire à tour sous sollicitations variables', thesis, University of Blida, February 2020.
[5]. BELHANI. A. Y and ABRAOUI. O., 'Conception et fabrication d'un héliostat pour une toure solaire', dissertation, Université Kasdi Merbah - Ouargla, 29 Mais 2017.
[6]. RAHMANI DJELLOUL, 'Analyse d'un système de concentration solaire pour la production d'hydrogène (cas de l'Algerie)', Dissertation, Univeristé Hassiba Benbouali de Chlef, 2012.
[7]. BELKACEM Mourad, 'Etude et optimisation du transfert d'énergie électrique en conversion photovoltaïque par la recherche du point de puissance maximal (MPPT)', Dissertation, Université Abou Belkaid de Tlemcen, 2015.
[8]. TABET Ismail. 'Etude, Réalisation et simulation d'un capteur solaire', thesis, Université des freres mentouri constantine, 2016.
[9]. TOUAFEK Khaled, Contribution à l'étude et à la conception d'un système énergétique utilisant des capteurs hybrides photovoltaïques thermiques, thesis, Ecole Normale Polytechnique ENP, Algeria, 2010.
[10]. S. Ben Mabrouk, 'Etude et Simulation d'un Capteur hybride Photovoltaique Thermique à air, University of Tunis El Manar, Researchgate, 2016.
[11]. Oussama El Manssouri, B. Hajji, Giuseppe M.T, Antonio G. and Stefano A., 'Electrical and Thermal Performances of Bi-Fluid PV/Thermal Collectors'. Energies 2021, 14, 1633.
[12]. Kamel Shalaoui, Hatem Oueslati & Salah Ben Mabrouk, 'Thermal and electrical performance evaluation of hybrid air PV/T collector - numerical analysis and experimental study', International journal of Sustainable Energy, 2021.
[13]. HAYIBO. K. S, 'Modélisation et simulation d'un capteur solaire hybride photovoltaïque thermique', Dissertation, Unversité Ouaga, 2016.
[14]. Khelifa Abdelkrim, 'Contribution à la conception et modélisation d'un capteur solaire hybride photovoltaïque thermique PVT', Thesis, Univertsité Hadj Lakhdar de Batna, 2017.
[15]. MEKADEM Hafsa and Mellouki H, 'Etude paramétrique d'un capteur hybride doté d'un concentrateur parabolique composé (PVT-CPC)', Dissertation, Université Ahmed Draia-Adrar, 2022.
[16]. Incropera, F.P.; DeWitt, D.P. Fundamentals of Heat and Mass Transfer, 6th ed; John Wiley & Sons, Inc: Hoboken, NJ, USA, 2007.
[17]. GHELLAB Amel, 'Modélisation et optimisation des capteurs solaires hybrides', thesis, Université des frères Mentours Constantine, 2018
[18]. A, Ghellab, A. Kaabi et al, 'Les retombées technico-économique d'un capteur hybride photovoltaïque/thermique à air', Revue des Energies Renouvelable Vol. 16 N°3 (2012) 425-550.
[19]. BOUHOREIRA Y. and GANA L. 'Etude de l'effet des paramètres sur les performances d'un collecteur solaire cylindro parabolique', dissertation, Université Kasdi Merbah Ouargla, 24-06-2018.
[20]. C. El Fouas, O. El Manssouri, B. Hajji et al, 'Study and Modeling of Energy performance of PV/T Solar Plant for Hydrogen Production', Engineering and Renewable Energy Systems, 2021.
[21]. Amina Benhammou. "Optimisation d'un nouveau système de séchage solaire modulaire pour plantes aromatiques et médicinales" thesis, University Abou Beker Belkaid, Algeria, Feb. 2010.
[22]. PASERA Joanès Keneddy, HARITHI BEN and DONA Victorien Bruno, "Optimizing the energy performance of a hybrid PVT air collector with Parabolic trough concentrator and Heliostat", IJARIIE-ISSN(O)-2395-4396, Vol-10 Issue-5 2024
[23]. HARITHI BEN Daoud Ben Attoumane, PASERA Joanès Keneddy and DONA Victorien Bruno, 'Energy performance studies of a PVT-air hybrid system with caes: influence of input parameters on the compression system', IJARIIE-ISSN(O)-2395-4396, Vol-10 Issue-4 2024
[24]. Ahed Hameed Jaaz, Husam A. H, Kamaruzzaman S.,Abdul Amir H. K., Tayser Sumer G. and Ahmed A. Al-Amiery , 'Outdoor Performance Analysis of a Photovoltaic Thermal (PVT) Collector with jet Impingement and Compound Parabolic Concentrator (CPC), Materials 2017, 10, 888.